MDPI

Article

Modeling of Combined Lead Fast Reactor and Concentrating Solar Power Supercritical Carbon Dioxide Cycles to Demonstrate Feasibility, Efficiency Gains, and Cost Reductions

Brian White [1], Michael Wagner [1,], Ty Neises[3], Cory Stansbury[4], and Ben Lindley [2]*

[1] Department of Mechanical Engineering, University of Wisconsin - Madison, 1415 University Drive, Madison, WI 53706, United States; dept@me.engr.wisc.edu
[2] Department of Engineering Physics, University of Wisconsin - Madison, 1500 Engineering Drive, Madison, WI 53706, United States; EMAIL
[3] National Renewable Energy Laboratory,Thermal Systems Group, 15013 Denver West Parkway, Golden, CO 80401, United States; EMAIL
[4] Westinghouse Electric Company, Lead Fast Reactor Systems Development, ADDRESS United States; EMAIL
* Correspondence: lindely2@wisc.edu (B.L); Tel.: +1-608-265-2001 (B.L.)

Abstract: Separate cycles for solar concentrating power (CSP) and lead-cooled fast reactors (LFRs), which innately have issues with weather, grid demand, and time of day, have potential to benefit when coupled together to a supercritical CO_2 Brayton cycle. Combining these cycles could allow for the LFR to thermally charge the salt storage in the solar concentrating power cycle during low demand periods and be utilized when grid demand increases. The LFR and CSP can use separate power conversion cycles or be combined into a single cycle. The LFR/CSP coupling into one cycle is modeled to find the preferred location of the LFR heat exchanger, CSP heat exchanger, salt charging heat exchanger, turbines, and recuperators within the supercritical CO_2 Brayton cycle. Three cycle configurations have been studied: a two-cycle configuration which uses CSP and LFR heat for dedicated turbocompressors, combined cycle with separate high temperature recuperators for both the CSP and LFR, and a combined cycle with CSP and LFR heat sources in parallel. [CONCLUSION]

Keywords: Supercritical carbon dioxide Brayton Cycle; Concentrating Solar Power (CSP); Lead Fast Reactor (LFR), Cogeneration, Combined Cycle, Thermal Energy Storage (TES)

Citation: White, B.; Lindley, B.; Wagner, M. Modeling of Combined Lead Fast Reactor and Concentrating Solar Power Supercritical Carbon Dioxide Cycles to Demonstrate Feasibility, Efficiency Gains, and Cost Reductions. *Sustainability* **2021**, *1*, 0. https://doi.org/

Received:
Accepted:
Published:

1. Introduction

2. Materials and Methods

2.1. Cycle Component Modeling

Components present in the cycles are modeled using various techniques. Turbines and compressors are analyzed using isentropic efficiencies. Counter flow heat exchangers use the effectiveness-NTU method while black box heat exchangers use a simple energy balance for state point calculations. The lead-cooled fast reactor is assumed to be a black box heat exchanger because of the constant heat input and state points on the sCO_2 inlet and outlet are provided. The concentrating solar power cycle is modeled with necessary components including hot and cold TES, reciever, pumps and counter flow heat exchangers.

2.1.1. Turbines and Compressors

The modeled cycles have a number of compressors and turbines. The turbines and compressors are modeled for each cycle using constant isentropic efficiency values summarized in Table 1. Turbines take the high pressure sCO_2 and expand it through a series of blades allowing a production of energy, while compressors input mechanical

energy to increase the pressure of the sCO_2. The turbines and compressors are assumed to be at steady state, exchange no heat with the surroundings, and have a single inlet and outlet. Power calculations are initially done on ideal, reversible compressors or turbines then are scaled by the isentropic efficiencies to provide an estimate for a realizable component. Using this estimate, along with a known low and high side pressures, temperature and enthalpy outlets of the turbine and compressor can be calculated [1].

2.1.2. Black Box and Counter Flow Heat Exchangers

Black box heat exchangers are simplified heat exchangers which have no approach temperature or pinch point. These heat exchangers use an energy balance with mass flow inlet energy, heat input or output, and mass flow outlet energy. The energy balance equation used for all black box heat exchangers is Equation 1.

$$\dot{m}_{in} * h_{in} + \dot{Q}_{in} = \dot{m}_{out} * h_{out} + \dot{Q}_{out}, \tag{1}$$

In this equation the energy input to the system is on the left hand side with $\dot{m}_{in}$ multiplied by h_{in} being energy from the mass flow and $\dot{Q}_{in}$ being heat transfer directly to the flow from an outside source. The right hand side of the equation is heat leaving the energy balance. The mass flow leaving is $\dot{m}_{out}$ with enthalpy of h_{out} and $\dot{Q}_{out}$ is the heat transfer leaving from the flow. Black box energy balances are used in three situations, the Reciever, LFR HX, and PC HX. These heat exchangers are not exchaustively modeled because the state points on the inlet and outlet are constrained by design parameters.

Counter flow heat exchangers are modeled with two fluids flowing in opposite directions exchanging heat from the hot side to the cold side. The temperatures of the hot and cold flows on either side of the the heat exchanger have a temperature difference known as an approach temperature. A diagram showing a simplified example of a counterflow heat exchanger is illustrated in Figure 1.

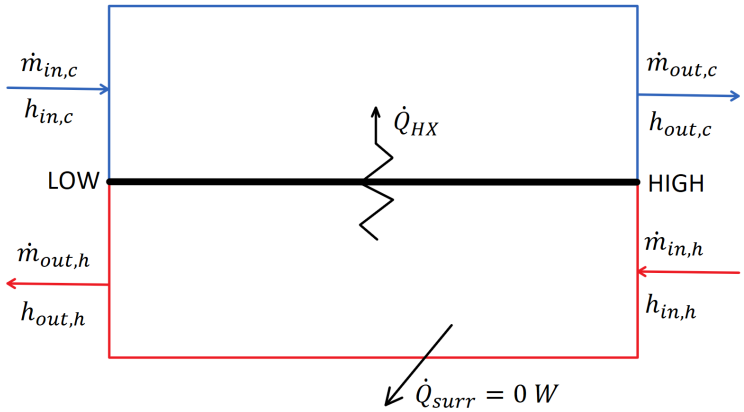

Figure 1. Simple counter flow heat exchanger diagram.

Additional assumptions of the counter flow heat exchanger model are no heat loss to the surroundings, $\dot{Q}_{surr}$ is zero, and no pressure drops accross the heat exchangers. Counter flow heat exchanger calculations require two known state points, fluid libraries, mass flow rate of hot and cold side, and a specified approach temperature. In all of the modeled cases, the approach temperature is set to a value of 10 K. The fluid libraries referenced are built into EES for Carbon Dioxide and Salt(60% NaNO3 40% KNO3) [2,3].

To analyze the counter flow heat exchanger a side is chosen, usually high, to start the calculations. The approach temperature is initially subtracted from the hot stream on the high side to find the missing cold temperature according to Equation 2.

$$T_{out,c} = T_{in,h} - \Delta_T, \tag{2}$$

Where $T_{out,c}$ is the cold stream outlet temperature and $T_{in,h}$ is the hot stream inlet temperature. Knowing the two state points allows for the enthalpy to be found using correlations from the fluid property libraries.

[More Desctription on Counterflow HX]

2.1.3. Lead-Cooled Fast Reactor

Lead-cooled fast reactors use energy from a controlled nuclear reaction to heat molten lead. This lead is used to both cool the core as well as transfer heat into the sCO_2 Brayton power cycle [4,5]. The lead-cooled fast reactor is assumed to be a black box heat transfer and is labeled in the cycle models LFR HX. The inlet, outlet and heat transfer rates are defined by our industry partner, Westinghouse Electric Company making the black box simplification viable. The energy balance for the black box assumption can be seen in Equation 3.

$$\dot{m}_{inlet} * h_{inlet} + \dot{Q}_{LFRHX} = \dot{m}_{outlet} * h_{outlet}, \tag{3}$$

Where the left hand side, $\dot{m}_{inlet}$, h_{inlet}, and $\dot{Q}_{LFRHX}$, is the energy into the flow and the right hand side, $\dot{m}_{outlet}$ and h_{outlet}, is the energy brought out from the flow of sCO_2. The amount of energy transfered into the cycle, $\dot{Q}_{LFRHX}$, is set at 950 MW, and outlet temperature of the sCO_2 from the LFR HX is set at a value of 595°C. The outlet temperature of the LFR is rigid due to high temperature material limits on the LFR lead side. Low sCO_2 LFR inlet temperature has a lower limit of 340°C and an optimal value of 400°C. Increasing this temperature above this optimal value leads to diminishing returns on the LFR efficiency.

2.1.4. Concentrating Solar Power Cycle

The CSP salt cycle modeled in this paper is composed of hot and cold thermal energy storage (TES), pumps, receiver, sCO_2-to-Salt counter flow heat exchanger (C2S), and CSP counter flow heat exchanger (CSP HX). The diagram for this CSP salt cycle is seen in Figure 2.

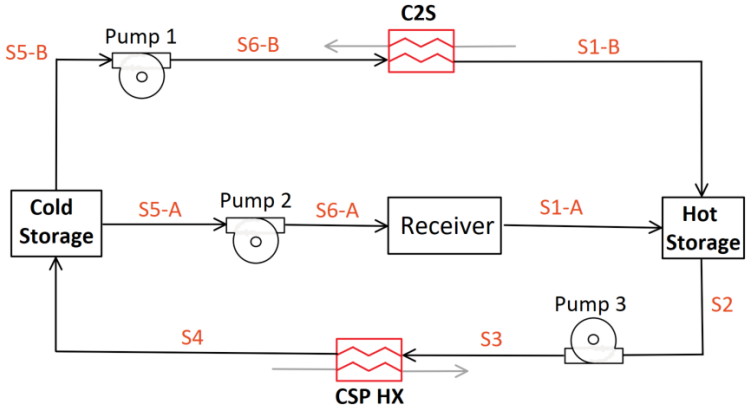

Figure 2. Diagram for CSP cycle with cold and hot thermal energy storage, pumps, and csp black box heat input

The CSP salt cycle uses 60% sodium nitrate and 40% potassium nitrate 'solar salt' as the heat transfer fluid. Solar salt stored in the hot TES can be dispatched on demand through the CSP HX when grid demand increases and held when grid demand is low. Current CSP salt cycles heat solar salt with receivers and store it in hot TES tanks at 565°C. Future CSP salt cycles are hypothesized to have bulk hot TES temperatures of up to 720°C, but due to high temperature limitations with the LFR outlet, the hot TES temperature is set at 595°C for all modeled cycles [6]. The cold TES temperature takes on three different values according to cycle configuration capabilitites: 390°C, 410°C, and 440°C. In addition to the lower hot TES temperature, current CSP salt cycles lack a

secondary option for charging the hot TES [7]. The studied CSP salt cycle has two TES charging options: a receiver, which generates heat from a heliostat field, and C2S heat exchanger, which draws excess heat from the sCO_2 Brayton cycle. It is assumed that only one hot TES charging option can be active at any given time.

The C2S heat exchanger is active during the 'charging' cycle configurations, when the focus is on heat storage for later use. During this process there is no solar salt flow through the receiver. Pump 1 is active moving solar salt from cold TES to hot TES through the C2S heat exchanger, which is extracting heat from the sCO_2 Brayton cycle.

'Non-charging' cycle configurations has the receiver charging the hot TES, C2S heat exchanger is not transfering heat, and the LFR is dispatching energy directly into electrical generation. When electrical generation is occuring, the heat input in this cycle is modelled through a black box energy balance across states S6-A and S1-A with a heat addition of 7.5e8 W from the heliostat field. The hot storage is moved through Pump 3 and transfers heat into the sCO_2 Brayton cycle to be converted into electricity. The cooled salt is stored in cold storage and moved through Pump 2 where the heat addition from the receiver is added.

2.2. Generalization of Cycle Modeling

The cycles presented are generalized in order to draw a more direct comparison. The generalized parameters include isentropic efficiencies, heat exchanger approach temperatures, pressures, heat input, and pump constants. These values are summarized in Table 1.

Table 1. Constant cycle parameters with definition, variable and set value.

Parameter	Variable	Design Point Value
Efficiencies		
Main Compressor	η_{MC}	0.91 (-)
Re-Compressor	η_{RC}	0.89 (-)
Turbine	η_T	0.90 (-)
Pump	η_P	0.90 (-)
Approach Temperatures		
Low Temperature Recuperator	δ_{LTR}	10 (K)
High Temperature Recuperator	δ_{HTR}	10 (K)
Concentrating Solar Power Heat Exchanger	δ_{CSPHX}	10 (K)
Pressures		
Pressure Ratio	PR	3.27 (-)
High Side Pressure	P_{2A}	2.88e7 (Pa)
Heat Into System		
Lead-Cooled Fast Reactor Heat Transfer	$\dot{Q}_{LFRHX}$	9.5e8 (W)
Concentrating Solar Power Heat Transfer	$\dot{Q}_{CSP}$	7.5e8 (W)
Temperature		
Main Compressor Inlet	T_{1A}	313.2 (K)
Lead-Cooled Fast Reactor sCO_2 High Temperature	T_5,T_{2C},T_{6A},T_{5C}	868.2 (K)
Pumps		
Pressure Rise Across Pump	Δ_P	3.726e6 (Pa)
Pump Low Side Pressure	P_{S5-B}	3.0e6 (Pa)

The values displayed in Table 1 are representative of LFR and CSP design while being consistent with design parameters given by our industry partner, Westinghouse Electric Company.

In addition to generalized parameters, all cycles have identical recompression sides. The recompression side contains a PreCooler, Low Temperature Recuperator, and two compressors; Main Compressor and ReCompressor.

Modeled cycles are summarized in Table 2.

Table 2. Summary of all modeled non-charging and charging cycles with descriptions.

Cycle Label	Description
Non-Charging	
C-LFR-ON	Two-cycle configuration with LFR as heat source.
C-CSP-ON	Two-cycle configuration with CSP as heat source.
C-1HTR1T-ON	CSP and LFR heat sources in parallel with one turbine.
C-2HTR3T-ON	Seperatre CSP and LFR loops each with dedicated HTR and turbine.
Charging	
C-LFR-PRE	Turbine is prior to the SALT HX.
C-LFR-POST	Turbine is after the SALT HX.
C-LFR-PAR	Turbine is parallel to the SALT HX.
C-LFR-CIRC	Circulator bridges the LFR and SALT HX.

2.3. Non-Charging Cycle Configurations

Various cycles are modeled to test their advantages and disadvantages. These cycle models fall into two categories: non-charging and charging. The non-charging category is used to determine the configuration of the cycle with a focus on electricity generation. This includes the number and location of turbines, recuperators, and heat input to the system by the CSP and LFR. To quantify the effectiveness of the non-charging configurations, a cycle efficiency, η_{cycle}, is defined in Equation 4.

$$\eta_{cycle} = \frac{\dot{W}_T - \dot{W}_{MC} - \dot{W}_{RC}}{\dot{Q}_{LFRHX} + \dot{Q}_{CSPHX}}, \tag{4}$$

The numerator in Equation 4 is the Alternator power, or the power produced from the turbines, $\dot{W}_T$, minus the required power of the compressors, $\dot{W}_{MC}$ and $\dot{W}_{RC}$. The denominator is the total power input into the system from the LFR HX, $\dot{Q}_{LFRHX}$, and CSP HX, $\dot{Q}_{CSPHX}$.

2.3.1. Two-Cycle Configuration: C-LFR-ON and C-CSP-ON

The two-cycle configuration that is tested has independent sCO_2 loops bridged by a CSP cycle. This cycle has two sCO_2 Brayton Cycles: C-LFR-ON and C-CSP-ON. Configuration of components for these two cycles is identical with the exception of heat inputs. C-LFR-ON has heat provided from a LFR while C-CSP-ON has heat provided from the CSP. These two cycles individually operate when the focus of plant operation is primarily electricity generation.

The cycle that is using the LFR heat input in the two-cycle configuration is labeled as C-LFR-ON and the cycle diagram is illustrated in Figure 3.

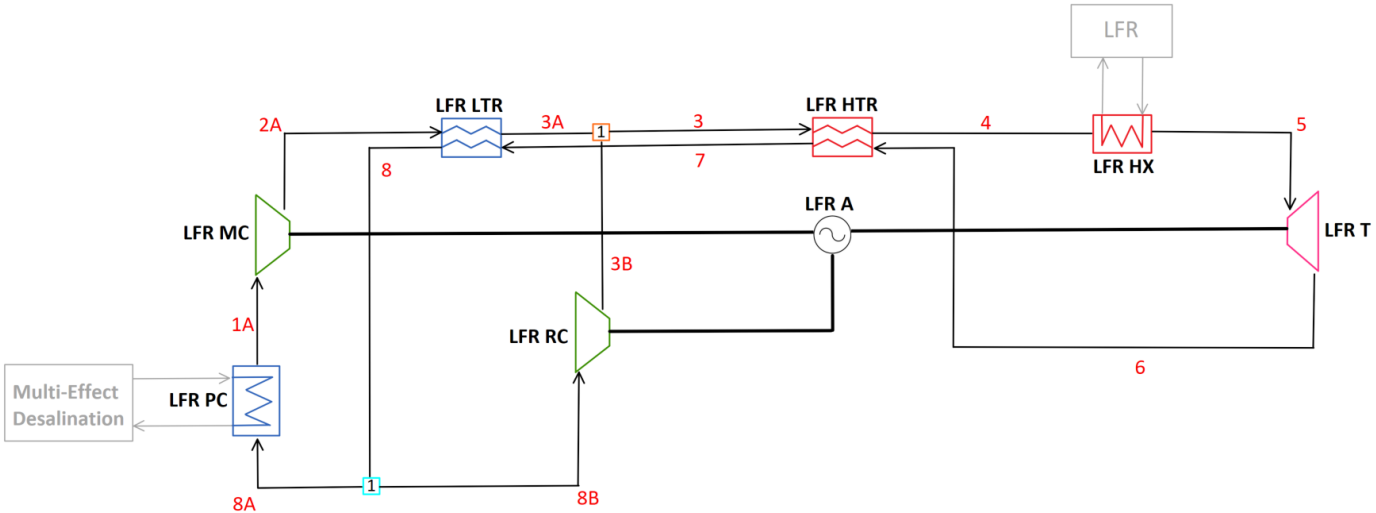

Two seperate sensitivity studies on the LFR inlet temperature are completed for C-LFR-ON. The unconstrained study is performed by gradually increasing the mass flow to the main compressor while maximizing cycle efficiency. The constrained study is calculated by setting the LFR inlet temperature to the design value of 673.2 K (400°C), which is a requirement of the LFR primary circuit to maximize power output within material limits.

The cycle that is using the CSP heat input in the two-cycle configuration is labeled C-CSP-ON and the cycle diagram is shown in Figure 4.

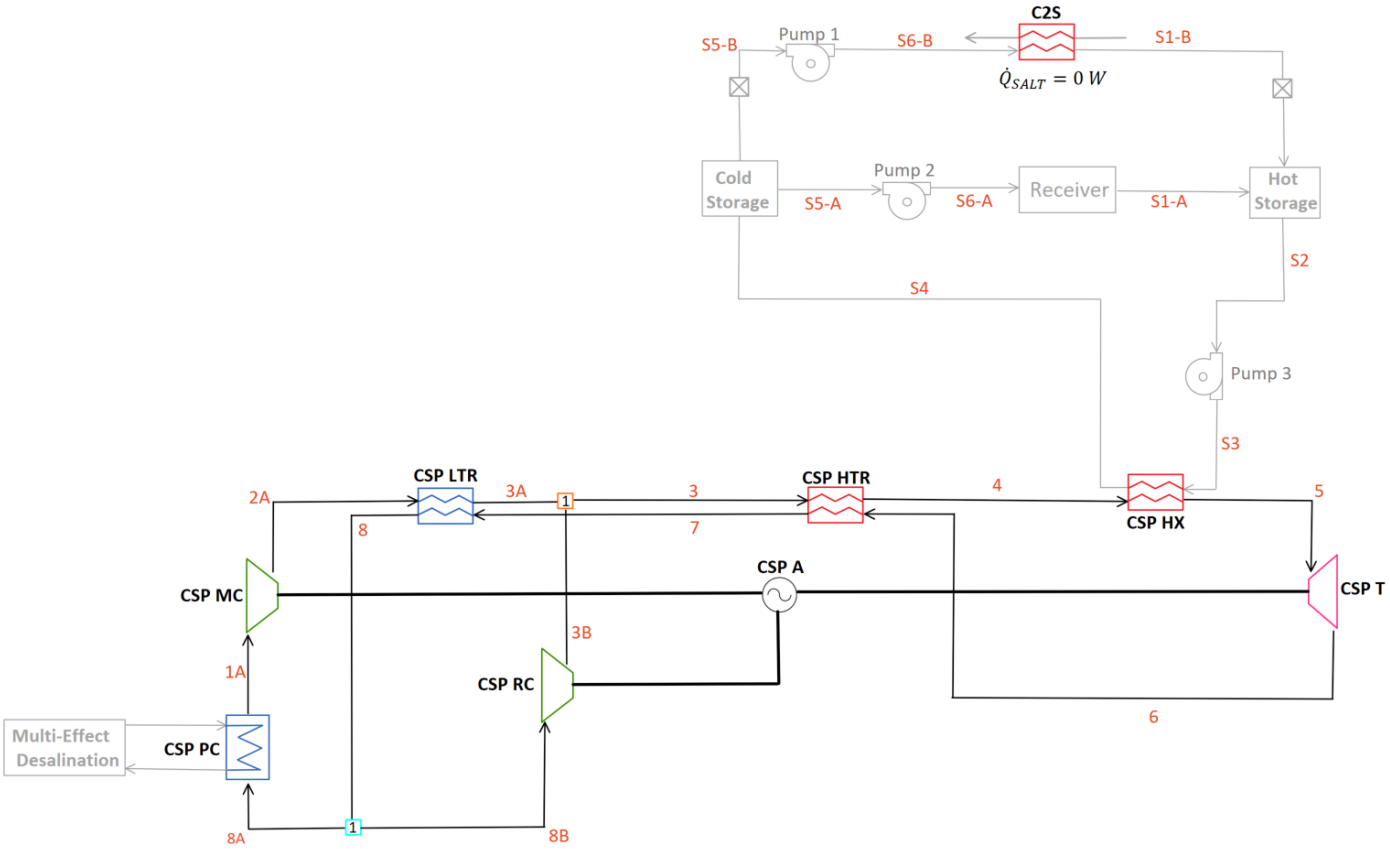

Figure 4. Diagram for C-CSP-ON with focus on electricity generation

Due to the individual operation while the cycles are generating electricity, C-CSP-ON is not directly impacted by the LFR low end temperatures. Instead, a sensitivity study is done on the temperature of the cold TES. Two temperatures are tested, 663.2 K and 713.2 K, to observe the impact of cold TES temperature on cycle efficiency.

2.3.2. C-1HTR1T-ON

One drawback of having a two-cycle design, as seen in the C-LFR-ON and C-CSP-ON, is doubling the number of system components. Combining the two cycles into one would reduce redundancy and complexity. Heat addition from the CSP HX and LFR HX in parallel orientation is therefore studied in the C-1HTR1T-ON model. This model studies what impact mixing different temperature flows prior to the turbine has on cycle efficiency. The diagram for this cycle is illustrated in Figure 5.

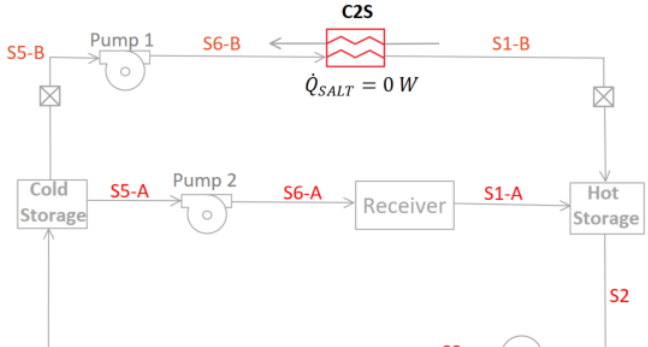

In this cycle, the LFR HX and CSP HX have identical inlet temperatures due to splitting the flow prior to their parallel orientation. Therefore, three sensitivity studies are done on the C-1HTR1T-ON EES model. The initial two studies have the low LFR temperature constrained to the value of 673.2 K with varied cold CSP TES and maximized cycle efficiency. The two tested values for cold CSP TES with constrained LFR low temperature are 683.2 K and 713.2 K. The desired cold CSP TES temperature of 663.2 K is not possible with the constraint on the LFR low temperature (because it cannot be colder than the sCO_2 that removes heat from the salt). In this case, to obtain the desired cold CSP TES temperature, the constraint on the LFR low temperature is removed, droping the temperature of the LFR inlet to 653.2 K.

2.3.3. C-2HTR3T-ON

Mixing two different temperature flows before the turbine in a Brayton cycle has a negative effect on cycle efficiency. To quantify the reduction in cycle efficiency, another cycle with no mixing prior to the turbine is desired. This cycle, C-2HTR3T-ON, can be seen in Figure 6 and has two high temperature recuperators and three turbines. The LFR is powering one turbine, T1, and recuperating heat through a dedicated high temperature recuperator, HTR1. The CSP cycle also contains two seperate turbines, T2, while having a dedicated high temperature recuperator, HTR2. After the high temperature recuperators, the two flows are combined and sent to the LTR hot side.

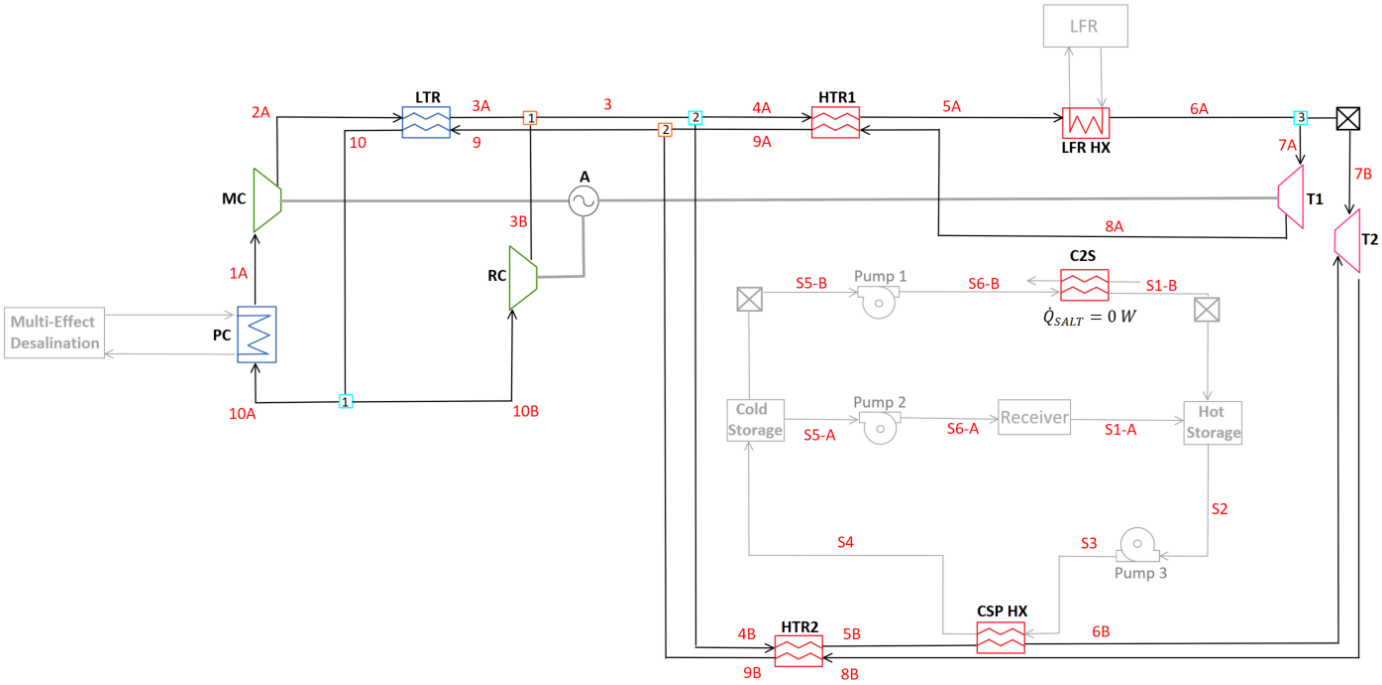

Figure 6. Diagram for C-2HTR3T-ON with focus on electricity generation

Three sensitivity studies are done on the C-2HTR3T-ON model. Two with the LFR low temperature constrained and one without this constraint. The two constrained studies had varied cold CSP TES temperature with the lowest temperature of 663.2 K and highest temperature of 713.2 K. The unconstrained low LFR inlet study is calculated at a cold CSP TES temperature of 663.2 K.

2.4. Thermal Energy Storage Charging Techniques

Charging cycle configurations focus on an energy storage operating mode. These configurations test the optimal location of LFR heat extraction through the SALT HX. To maximize the available heat for extraction, alternator power is set to zero and turbine power is therefore equal to the compressors' demand. The excess energy from the LFR

is thermally stored in the TES for later use when grid demand increases. Comparison of where thermal energy is extracted in the cycle is done by using the same Brayton cycle, C-LFR-ON, and configuring the salt heat exchanger in different locations around the turbine. To quantify the effectiveness of TES charging techniques a heat storage efficiency, $\eta_{heatstorage}$, is defined by Equation 5.

$$\eta_{heatstorage} = \frac{\dot{Q}_{C2S}}{\dot{Q}_{LFRHX} + \dot{Q}_{CSPHX}}, \tag{5}$$

Whereas $\dot{Q}_{S2C}$ is the amount of heat transfered through S2C and the addition of $\dot{Q}_{LFRHX}$ and $\dot{Q}_{CSPHX}$ is the total amount of heat input into the system from the LFR HX and CSP HX.

2.4.1. C-LFR-PRE

Flow leaving the turbine contains excess thermal energy that is not transformed into electrical energy. This excess thermal energy is stored in the hot CSP TES. The diagram outlining this process is C-LFR-PRE in Fig. 7.

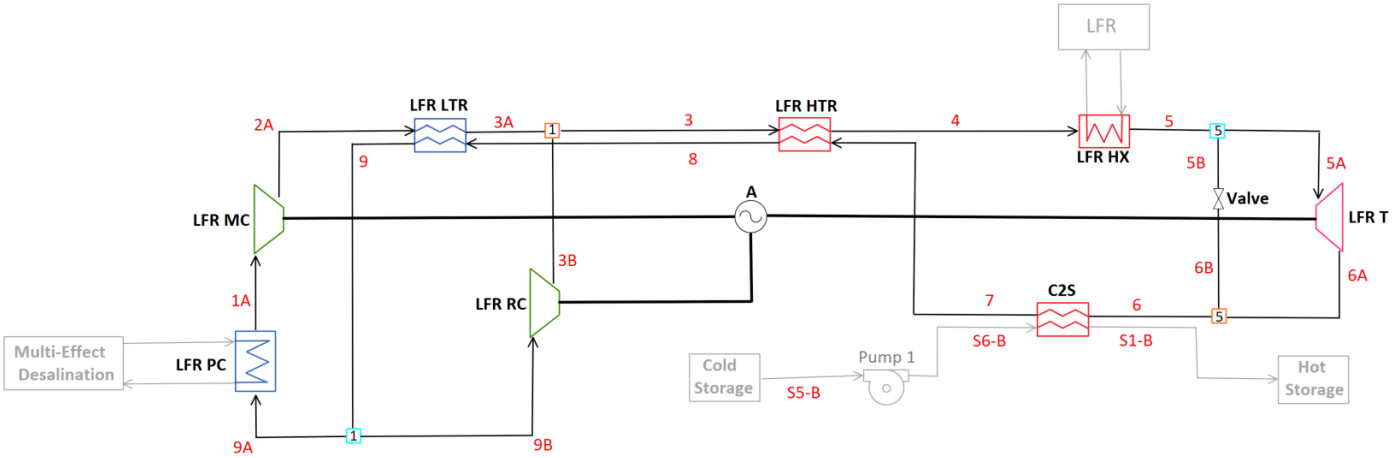

Figure 7. Diagram for C-LFR-PRE thermal energy storage charging orientation

Problems arise with this salt charging configuration. The temperature out of the turbine is not high enough to charge the hot CSP TES to the required value of 833.2 K. To raise the temperature, some of the high temperature flow before the turbine is redirected through a valve and combined after the turbine. Combining different temperature flows and reducing the flow through the turbine has a large impact on heat storage efficiency.

2.4.2. C-LFR-POST

Moving the heat extraction prior to the turbine is analyzed in C-LFR-POST. This diagram is seen in Figure 8.

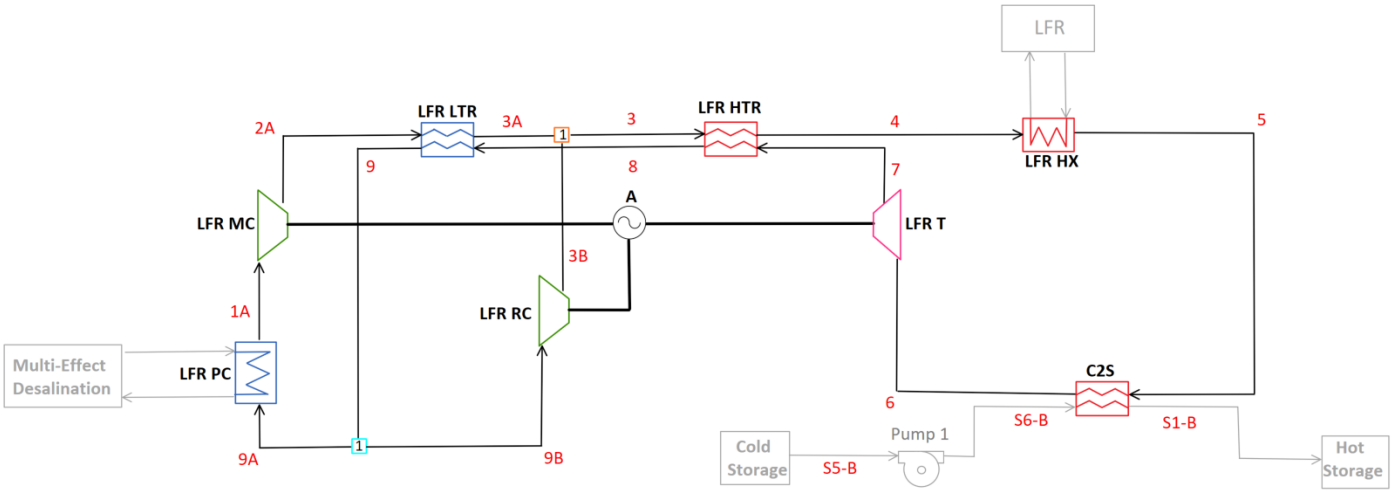

Figure 8. Diagram for C-LFR-POST thermal energy storage charging orientation

This TES charging cycle extracts heat before the turbine and therefore would have a large negative effect on the amount of work that the turbine could produce. The turbine needs to offset the requirements of both compressors and this would require the inlet temperature to be high. The amount of energy that could be extracted before the turbine would be small and therefore the heat storage efficiency would be small. There is no quantitative study done on this case because, due to the efficiency losses, it is non-viable.

2.4.3. C-LFR-PAR

The requirement of the turbine and CSP hot TES temperature can be accomplished by splitting the flow before the turbine. The flow through the salt heat exchanger in this cycle is therefore seperate from the turbine. After the salt heat exchanger a valve is needed to reduce the pressure, this TES charging cycle is C-LFR-PAR shown in Figure 9.

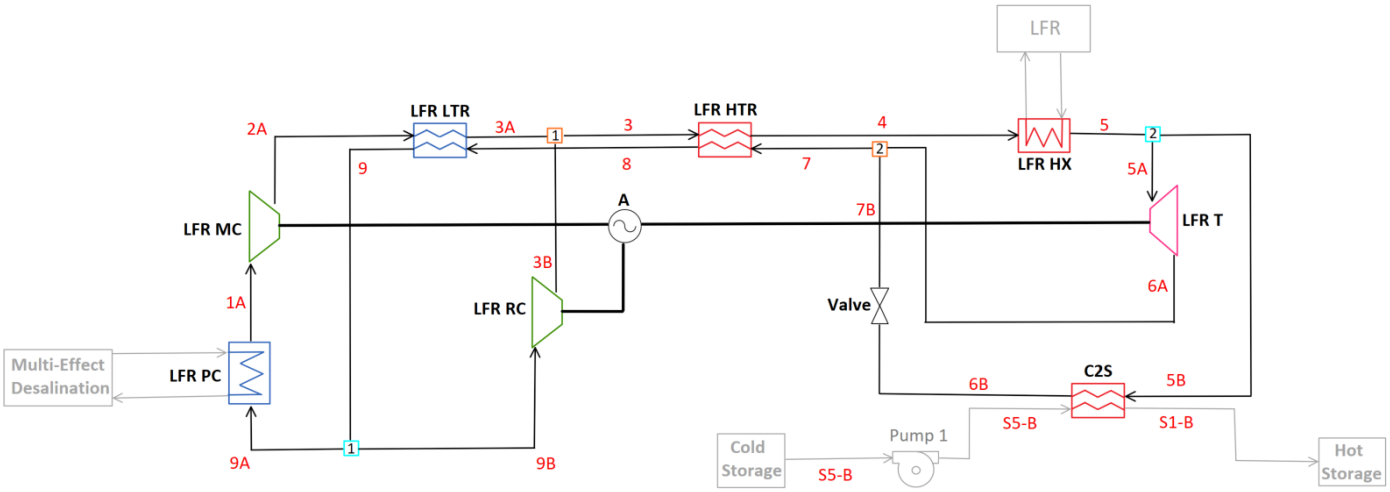

Figure 9. Diagram for C-LFR-PAR thermal energy storage charging orientation

Two sensitivity studies with varying cold CSP TES are desired to see the impact on heat storage efficiency. The TES temperature study is calculated with a low TES temperature of 663.2 K and a high TES temperature of 713.2 K.

2.4.4. C-LFR-CIRC

The full diagram for C-LFR-CIRC is shown in Figure 10.

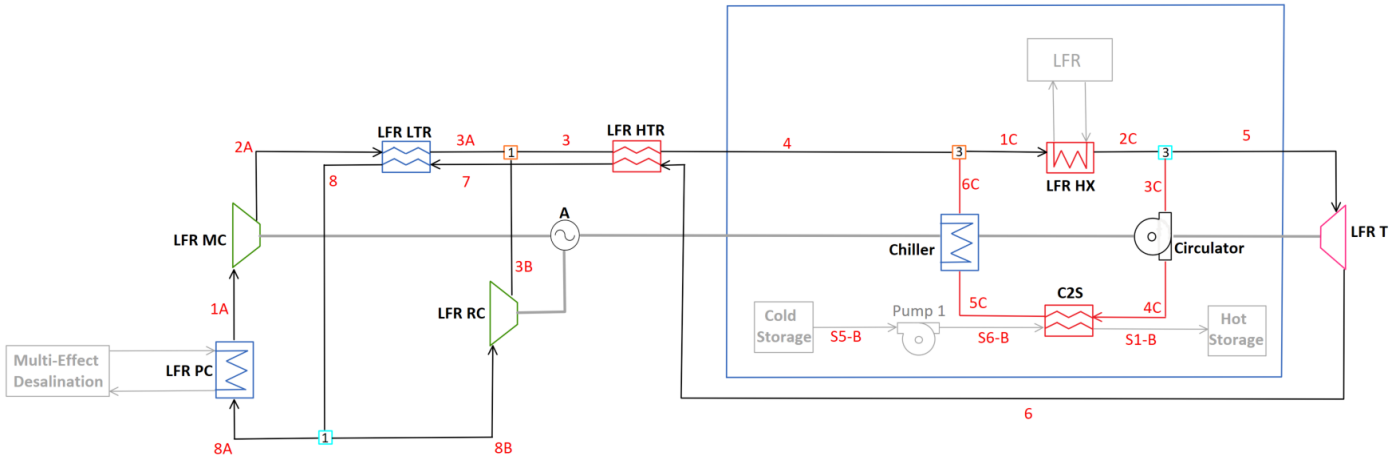

Figure 10. Full diagram for C-LFR-CIRC thermal energy storage charging orientation

The charging subsection of this diagram is composed of a circulation cycle that has heat inputed through the LFR heat exchanger. This subsection is encircled in blue and can be seen in Figure 11.

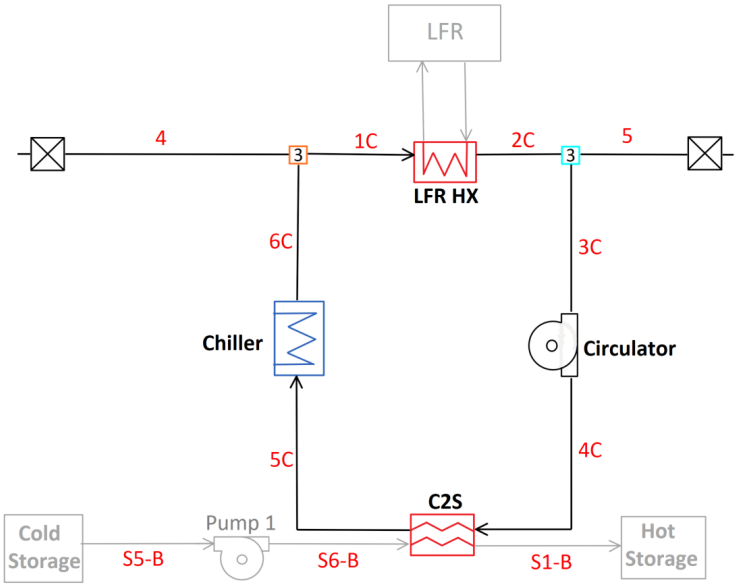

Figure 11. Diagram for C-LFR-CIRC subcycle thermal energy storage charging orientation

The flow continues through a circulator which is assumed to have neglegible pressure rise (i.e. there is assumed to be negligible pressure drop in this case). A heat exchanger, SALT HX, extracts heat from the flow, storing the thermal energy in the hot TES for later use. Excess heat that is not extracted is then dumped into a reservior through the chiller to bring the temperature of the flow down to LFR cool side operating temperature of 673.2 K. Three different temperatures; 663.2 K, 683.2 K, and 713.2 K, are compared in a sensitivity study.

3. Results

3.1. Non-Charging Cycle Configurations

3.1.1. C-LFR-ON and C-CSP-ON

Modeling the C-LFR-ON cycle in EES yeilded the results in Table 3.

Table 3. Calculated system parameters for non-charging C-LFR-ON cycle configuration with constrained (*C*) and unconstrained (*U*) lead-cooled fast reactor low-end temperature.

Definition	**Variable**	*U*	*C*
LFR Inlet Temperature (K)	T_4	Data	Data
Cycle Efficiency (%)	η_{cycle}	Data	Data
Alternator Power (W)	$\dot{W}_A$	Data	Data
PC Heat Transfer	$\dot{Q}_{PC}$	Data	Data
MC Power (W)	$\dot{W}_{MC}$	Data	Data
RC Power (W)	$\dot{W}_{RC}$	Data	Data
Turbine Power (W)	$\dot{W}_T$	Data	Data
MC Mass Flow Fraction (-)	y_1	Data	Data
LTR UA Value (W/K)	UA_{LTR}	Data	Data
LTR Capacitance Ratio (-)	CR_{LTR}	Data	Data
LTR Heat Transfer Rate (W)	$\dot{Q}_{LTR}$	Data	Data
LTR Effectiveness (-)	ε_{LTR}	Data	Data
HTR UA Value (W/K)	UA_{HTR}	Data	Data
HTR Capacitance Ratio (-)	CR_{HTR}	Data	Data
HTR Heat Transfer Rate (W)	$\dot{Q}_{HTR}$	Data	Data
HTR Effectiveness (-)	ε_{HTR}	Data	Data

Discussion of Results

The EES model outputs for C-CSP-ON are listed in Table 4.

Table 4. Calculated system parameters for non-charging C-CSP-ON cycle configuration with varied TES cold temperature.

Definition	**Variable**		
Cold TES Temperature (K)	T_{CS}	Data	Data
Cycle Efficiency (%)	η_{cycle}	Data	Data
Alternator Power (W)	$\dot{W}_A$	Data	Data
PC Heat Transfer	$\dot{Q}_{PC}$	Data	Data
MC Power (W)	$\dot{W}_{MC}$	Data	Data
RC Power (W)	$\dot{W}_{RC}$	Data	Data
Turbine Power (W)	$\dot{W}_T$	Data	Data
MC Mass Flow Fraction (-)	y_1	Data	Data
LTR UA Value (W/K)	UA_{LTR}	Data	Data
LTR Capacitance Ratio (-)	CR_{LTR}	Data	Data
LTR Heat Transfer Rate (W)	$\dot{Q}_{LTR}$	Data	Data
LTR Effectiveness (-)	ε_{LTR}	Data	Data
HTR UA Value (W/K)	UA_{HTR}	Data	Data
HTR Capacitance Ratio (-)	CR_{HTR}	Data	Data
HTR Heat Transfer Rate (W)	$\dot{Q}_{HTR}$	Data	Data
HTR Effectiveness (-)	ε_{HTR}	Data	Data
CSPHX UA Value (W/K)	UA_{CSPHX}	Data	Data
CSPHX Capacitance Ratio (-)	CR_{CSPHX}	Data	Data
CSPHX Heat Transfer Rate (W)	$\dot{Q}_{CSPHX}$	Data	Data
CSPHX Effectiveness (-)	ε_{CSPHX}	Data	Data

Discussion of Results

3.1.2. C-1HTR1T-ON

These values are displayed in Table 5.

Table 5. Calculated system parameters for non-charging C-1HTR1T-ON cycle configuration with constrained (*C*) and unconstrained (*U*) lead-cooled fast reactor low-end temperature. Temperature of TES cold temperature is also varied.

Definition	**Variable**	**C-1HTR1T-ON**		
		U	*C*	*C*
Cold TES Temperature (K)	T_{CS}	Data	Data	Data
LFR Inlet Temperature (K)	T_{4C}	Data	Data	Data
Cycle Efficiency (%)	η_{cycle}	Data	Data	Data
Alternator Power (W)	$\dot{W}_A$	Data	Data	Data
PC Heat Transfer	$\dot{Q}_{PC}$	Data	Data	Data
MC Power (W)	$\dot{W}_{MC}$	Data	Data	Data
RC Power (W)	$\dot{W}_{RC}$	Data	Data	Data
Turbine Power (W)	$\dot{W}_T$	Data	Data	Data
MC Mass Flow Fraction (-)	y_1	Data	Data	Data
LFR Mass Flow Fraction (-)	y_2	Data	Data	Data
LTR UA Value (W/K)	UA_{LTR}	Data	Data	Data
LTR Capacitance Ratio (-)	CR_{LTR}	Data	Data	Data
LTR Heat Transfer Rate (W)	$\dot{Q}_{LTR}$	Data	Data	Data
LTR Effectiveness (-)	ε_{LTR}	Data	Data	Data
HTR UA Value (W/K)	UA_{HTR}	Data	Data	Data
HTR Capacitance Ratio (-)	CR_{HTR}	Data	Data	Data
HTR Heat Transfer Rate (W)	$\dot{Q}_{HTR}$	Data	Data	Data
HTR Effectiveness (-)	ε_{HTR}	Data	Data	Data
CSPHX UA Value (W/K)	UA_{CSPHX}	Data	Data	Data
CSPHX Capacitance Ratio (-)	CR_{CSPHX}	Data	Data	Data
CSPHX Heat Transfer Rate (W)	$\dot{Q}_{CSPHX}$	Data	Data	Data
CSPHX Effectiveness (-)	ε_{CSPHX}	Data	Data	Data

Discussion of Results

3.1.3. C-2HTR3T-ON

The calculated values from these studies are displayed in Table 6.

Table 6. Calculated system parameters for non-charging C-2HTR3T-ON cycle configuration with constrained (*C*) and unconstrained (*U*) lead-cooled fast reactor low-end temperature.

Definition	**Variable**	**C-2HTR3T-ON**		
		U	*C*	*C*
Cold TES Temperature (K)	T_{CS}	Data	Data	Data
LFR Inlet Temperature (K)	T_{5A}	Data	Data	Data
Cycle Efficiency (%)	η_{cycle}	Data	Data	Data
Alternator Power (W)	$\dot{W}_A$	Data	Data	Data
PC Heat Transfer	$\dot{Q}_{PC}$	Data	Data	Data
MC Power (W)	$\dot{W}_{MC}$	Data	Data	Data
RC Power (W)	$\dot{W}_{RC}$	Data	Data	Data
T1 Power (W)	$\dot{W}_{T1}$	Data	Data	Data
T2 Power (W)	$\dot{W}_{T2}$	Data	Data	Data
MC Mass Flow Fraction (-)	y_1	Data	Data	Data
LFR Mass Flow Fraction (-)	y_2	Data	Data	Data
LTR UA Value (W/K)	UA_{LTR}	Data	Data	Data
LTR Capacitance Ratio (-)	CR_{LTR}	Data	Data	Data
LTR Heat Transfer Rate (W)	$\dot{Q}_{LTR}$	Data	Data	Data
LTR Effectiveness (-)	ε_{LTR}	Data	Data	Data
HTR1 UA Value (W/K)	UA_{HTR1}	Data	Data	Data
HTR1 Capacitance Ratio (-)	CR_{HTR1}	Data	Data	Data
HTR1 Heat Transfer Rate (W)	$\dot{Q}_{HTR1}$	Data	Data	Data
HTR1 Effectiveness (-)	ε_{HTR1}	Data	Data	Data
HTR2 UA Value (W/K)	UA_{HTR2}	Data	Data	Data
HTR2 Capacitance Ratio (-)	CR_{HTR2}	Data	Data	Data
HTR2 Heat Transfer Rate (W)	$\dot{Q}_{HTR2}$	Data	Data	Data
HTR2 Effectiveness (-)	ε_{HTR2}	Data	Data	Data
CSPHX UA Value (W/K)	UA_{CSPHX}	Data	Data	Data
CSPHX Capacitance Ratio (-)	CR_{CSPHX}	Data	Data	Data
CSPHX Heat Transfer Rate (W)	$\dot{Q}_{CSPHX}$	Data	Data	Data
CSPHX Effectiveness (-)	ε_{CSPHX}	Data	Data	Data

Discussion of Results

3.2. Thermal Energy Storage Charging Techniques

3.2.1. C-LFR-PRE

The calculations from this TES charging technique are shown in Table 7.

Table 7. Calculated system parameters for salt charging C-LFR-PRE cycle configuration with TES cold storage set to 663.2 K.

Definition	**Variable**	**C-LFR-PRE** *C*
Cold TES Temperature (K)	T_{CS}	Data
LFR Inlet Temperature (K)	T_4	Data
Heat Storage Efficiency (%)	$\eta_{heatstorage}$	Data
Alternator Power (W)	$\dot{W}_A$	Data
PC Heat Transfer	$\dot{Q}_{PC}$	Data
MC Power (W)	$\dot{W}_{MC}$	Data
RC Power (W)	$\dot{W}_{RC}$	Data
Turbine Power (W)	$\dot{W}_T$	Data
MC Mass Flow Fraction (-)	y_1	Data
Valve Mass Flow Fraction (-)	y_5	Data
LTR UA Value (W/K)	UA_{LTR}	Data
LTR Capacitance Ratio (-)	CR_{LTR}	Data
LTR Heat Transfer Rate (W)	$\dot{Q}_{LTR}$	Data
LTR Effectiveness (-)	ε_{LTR}	Data
HTR UA Value (W/K)	UA_{HTR}	Data
HTR Capacitance Ratio (-)	CR_{HTR}	Data
HTR Heat Transfer Rate (W)	$\dot{Q}_{HTR}$	Data
HTR Effectiveness (-)	ε_{HTR}	Data
CSPHX UA Value (W/K)	UA_{CSPHX}	Data
CSPHX Capacitance Ratio (-)	CR_{CSPHX}	Data
CSPHX Heat Transfer Rate (W)	$\dot{Q}_{CSPHX}$	Data
CSPHX Effectiveness (-)	ε_{CSPHX}	Data

Discussion of Results

3.2.2. C-LFR-POST

3.2.3. C-LFR-PAR

The results from this study are displayed in Table 8.

Table 8. Calculated system parameters for salt charging C-LFR-PAR cycle configuration with TES cold storage varied and LFR low temperature set to 673.2 K.

Definition	**Variable**	**C-2HTR3T-ON**	
		C	*C*
Cold TES Temperature (K)	T_{CS}	Data	Data
LFR Inlet Temperature (K)	T_4	Data	Data
Heat Storage Efficiency (%)	$\eta_{heatstorage}$	Data	Data
Alternator Power (W)	$\dot{W}_A$	Data	Data
PC Heat Transfer	$\dot{Q}_{PC}$	Data	Data
MC Power (W)	$\dot{W}_{MC}$	Data	Data
RC Power (W)	$\dot{W}_{RC}$	Data	Data
Turbine Power (W)	$\dot{W}_T$	Data	Data
MC Mass Flow Fraction (-)	y_1	Data	Data
SALT HX Mass Flow Fraction (-)	y_2	Data	Data
LTR UA Value (W/K)	UA_{LTR}	Data	Data
LTR Capacitance Ratio (-)	CR_{LTR}	Data	Data
LTR Heat Transfer Rate (W)	$\dot{Q}_{LTR}$	Data	Data
LTR Effectiveness (-)	ε_{LTR}	Data	Data
HTR UA Value (W/K)	UA_{HTR}	Data	Data
HTR Capacitance Ratio (-)	CR_{HTR}	Data	Data
HTR Heat Transfer Rate (W)	$\dot{Q}_{HTR}$	Data	Data
HTR Effectiveness (-)	ε_{HTR}	Data	Data
CSPHX UA Value (W/K)	UA_{CSPHX}	Data	Data
CSPHX Capacitance Ratio (-)	CR_{CSPHX}	Data	Data
CSPHX Heat Transfer Rate (W)	$\dot{Q}_{CSPHX}$	Data	Data
CSPHX Effectiveness (-)	ε_{CSPHX}	Data	Data
CSPHX Approach Temperature (K)	δ_{CSPHX}	Data	Data

Changing the temperature of the cold CSP TES had little effect on the heat storage efficiency. The CSP salt mass flow rate and approach temperature of the SALT HX would adjust according to the temperature difference in the TES and keep the efficiency constant.

3.2.4. C-LFR-CIRC

Table 9 to show cold thermal energy storage's affect on heat storage efficiency.

Table 9. Calculated system parameters for charging C-LFR-CIRC subcycle configuration with constrained lead-cooled fast reactor low-end temperature.

Definition	**Variable**	**C-LFR-CIRC**		
Cold TES Temperature (K)	T_{CS}	Data	Data	Data
LFR Inlet Temperature (K)	T_{1C}	Data	Data	Data
Heat Storage Efficiency (%)	$\eta_{heatstorage}$	Data	Data	Data
Chiller Heat Transfer (W)	$\dot{Q}_{chill}$	Data	Data	Data
CSPHX UA Value (W/K)	UA_{CSPHX}	Data	Data	Data
CSPHX Capacitance Ratio (-)	CR_{CSPHX}	Data	Data	Data
CSPHX Heat Transfer Rate (W)	$\dot{Q}_{CSPHX}$	Data	Data	Data
CSPHX Effectiveness (-)	ε_{CSPHX}	Data	Data	Data

4. Discussion

Authors should discuss the results and how they can be interpreted from the perspective of previous studies and of the working hypotheses. The findings and their implications should be discussed in the broadest context possible. Future research directions may also be highlighted.

5. Conclusions

This section is not mandatory, but can be added to the manuscript if the discussion is unusually long or complex.

6. how to use

6.1. Subsection

Citing a journal paper [8] . Now citing a book reference [9] or other reference types [10]. [11]

6.1.1. Subsubsection

Bulleted lists look like this:

- First bullet;
- Second bullet;
- Third bullet.

Numbered lists can be added as follows:

1. First item;
2. Second item;
3. Third item.

The text continues here.

6.2. Figures, Tables and Schemes

All figures and tables should be cited in the main text as Figure 12, Table 10, etc.

Figure 12. This is a figure. Schemes follow the same formatting. If there are multiple panels, they should be listed as: (**a**) Description of what is contained in the first panel. (**b**) Description of what is contained in the second panel. Figures should be placed in the main text near to the first time they are cited. A caption on a single line should be centered.

Table 10. This is a table caption. Tables should be placed in the main text near to the first time they are cited.

Title 1	Title 2	Title 3
Entry 1	Data	Data
Entry 2	Data	Data

Text.
Text.

6.3. Formatting of Mathematical Components

This is the example 1 of equation:

$$a = 1, \tag{6}$$

the text following an equation need not be a new paragraph. Please punctuate equations as regular text.

This is the example 2 of equation:

$$\begin{aligned} a &= b + c + d + e + f + g + h + i + j + k + l \\ &+ m + n + o + p + q + r + s + t + u + v + w + x + y + z \end{aligned} \tag{7}$$

Please punctuate equations as regular text. Theorem-type environments (including propositions, lemmas, corollaries etc.) can be formatted as follows:

Theorem 1. *Example text of a theorem.*

The text continues here. Proofs must be formatted as follows:

Proof of Theorem 1. Text of the proof. Note that the phrase "of Theorem 1" is optional if it is clear which theorem is being referred to. □

The text continues here.

Author Contributions: For research articles with several authors, a short paragraph specifying their individual contributions must be provided. The following statements should be used "Conceptualization, X.X. and Y.Y.; methodology, X.X.; software, X.X.; validation, X.X., Y.Y. and Z.Z.; formal analysis, X.X.; investigation, X.X.; resources, X.X.; data curation, X.X.; writing—original draft preparation, X.X.; writing—review and editing, X.X.; visualization, X.X.; supervision, X.X.; project administration, X.X.; funding acquisition, Y.Y. All authors have read and agreed to the published version of the manuscript.", please turn to the CRediT taxonomy for the term explanation. Authorship must be limited to those who have contributed substantially to the work reported.

Funding: Please add: "This research received no external funding" or "This research was funded by NAME OF FUNDER grant number XXX." and and "The APC was funded by XXX". Check carefully that the details given are accurate and use the standard spelling of funding agency names at https://search.crossref.org/funding, any errors may affect your future funding.

Data Availability Statement: In this section, please provide details regarding where data supporting reported results can be found, including links to publicly archived datasets analyzed or generated during the study. Please refer to suggested Data Availability Statements in section "MDPI Research Data Policies" at https://www.mdpi.com/ethics. You might choose to exclude this statement if the study did not report any data.

Acknowledgments: In this section you can acknowledge any support given which is not covered by the author contribution or funding sections. This may include administrative and technical support, or donations in kind (e.g., materials used for experiments).

Conflicts of Interest: Declare conflicts of interest or state "The authors declare no conflict of interest." Authors must identify and declare any personal circumstances or interest that may be perceived as inappropriately influencing the representation or interpretation of reported research results. Any role of the funders in the design of the study; in the collection, analyses or interpretation of data; in the writing of the manuscript, or in the decision to publish the results must be declared in this section. If there is no role, please state "The funders had no role in the design of the study; in the collection, analyses, or interpretation of data; in the writing of the manuscript, or in the decision to publish the results".

Nomenclature

The following abbreviations and variables are used in this manuscript:

Abbreviations:

A	Alternator
CSP	Concentrating solar power
C2S	sCO_2-to-Salt heat exchanger
EES	Engineering Equation Solver
HTR	High temperature recuperator
HX	Heat exchanger
LFR	Lead-fast reactor
LTR	Low temperature recuperator
MC	Main compressor
NREL	National Renewable Energy Laboratory
P	Pump
PC	Pre-cooler
RC	Re-compressor
sCO_2	Supercritical carbon dioxide
T	Turbine
TES	Thermal energy storage

Variables [Units]:

CR	Capacitance Ratio [-]
$\dot{C}$	Capacitance Rate [W/K]
Δ	Temperature difference [K]
δ	Approach temperature of heat exchanger [K]
ε	Effectiveness of heat exchanger [-]
η	Isentropic efficiency [-]
h	Enthalpy [J/kg]
$\dot{m}$	Mass flow rate [kg/s]
NTU	Number of transfer units [-]
P	Pressure [Pa]
$\dot{Q}$	Heat transfer rate [W]
T	Temperature [K]
UA	Conductivity of heat exchanger [W/K]
v	Volumetric flow rate [m^3/kg]
$\dot{W}$	Power [W]
y	Splitter Fraction [-]

```
#My ees file
def myfunc():
    return x
x = y

f = 8*y^2
```

$$a^2 + b^2 = c^2 \tag{8}$$

References

1. Klein, S.; Nellis, G. *Thermodynamics*; Cambridge University Press, 2011. doi:10.1017/CBO9780511994883.
2. Pacheco, J.E.; Ralph, M.E.; Chavez, J.M.; Dunkin, S.R.; Rush, E.E.; Ghanbari, C.M.; Matthews, M.W. Results of molten salt panel and component experiments for solar central receivers: Cold fill, freeze/thaw, thermal cycling and shock, and instrumentation tests **1995**. doi:10.2172/46671.
3. Span, R.; Wagner, W. A New Equation of State for Carbon Dioxide Covering the Fluid Region from the Triple-Point Temperature to 1100 K at Pressures up to 800 MPa. *Journal of Physical and Chemical Reference Data* **1996**, *25*, 1509–1596, [https://doi.org/10.1063/1.555991]. doi:10.1063/1.555991.
4. Smith, C.; Cinotti, L. 6 - Lead-cooled fast reactor. In *Handbook of Generation IV Nuclear Reactors*; Pioro, I.L., Ed.; Woodhead Publishing Series in Energy, Woodhead Publishing, 2016; pp. 119–155. doi:https://doi.org/10.1016/B978-0-08-100149-3.00006-9.

5. Alemberti, A.; Smirnov, V.; Smith, C.F.; Takahashi, M. Overview of lead-cooled fast reactor activities. *Progress in Nuclear Energy* **2014**, *77*, 300–307. doi:https://doi.org/10.1016/j.pnucene.2013.11.011.
6. Mehos, M.; Turchi, C.; Vidal, J.; Wagner, M.; Ma, Z.; Ho, C.; Kolb, W.; Andraka, C.; Kruizenga, A. Concentrating solar power Gen3 demonstration roadmap. Technical report, National Renewable Energy Lab.(NREL), Golden, CO (United States), 2017.
7. Hamilton, W.T.; Husted, M.A.; Newman, A.M.; Braun, R.J.; Wagner, M.J. Dispatch optimization of concentrating solar power with utility-scale photovoltaics. *Optimization and Engineering* **2020**, *21*, 335–369.
8. Wagner, M.J. Optimization of stored energy dispatch for concentrating solar power systems. PhD thesis, Colorado School of Mines, 2017.
9. Blair, N.; Dobos, A.; Freeman, J.; Gilman, P.; Janzou, P.; Wagner, M.; Neises, T.; Mehos, M. SAM five year solar technologies roadmap. *Applied energy* **2005**, *231*, 1109–1121.
10. Hirsch, T.; Eck, M.; Blanco, M.J.; Wagner, M.; Feldhoff, J.F. Standardization of CSP Performance Model Projection: Latest Results From the guiSmo Project. Energy Sustainability, 2011, Vol. 54686, pp. 737–742.
11. Nellis, G.; Klein, S. *Heat Transfer*; Cambridge University Press, 2008. doi:10.1017/CBO9780511841606.